Breakdown of topological protection due to nonmagnetic edge disorder in two-dimensional materials in the quantum spin Hall phase

Leandro R. F. Lima[1] and Caio Lewenkopf[2,3]

[1]*Departamento de Física, Instituto de Ciências Exatas, Universidade Federal Rural do Rio de Janeiro, 23897-000 Seropédica, RJ, Brazil*

[2]*Instituto de Física, Universidade Federal Fluminense, 24210-346 Niterói, RJ, Brazil*

[3]*Max Planck Institute for the Physics of Complex Systems, 01187 Dresden, Germany*

(Received 1 July 2022; revised 7 October 2022; accepted 17 November 2022; published 7 December 2022)

We study the suppression of the conductance quantization in quantum spin Hall systems by a combined effect of electronic interactions and edge disorder, that is ubiquitous in exfoliated and chemical vapor deposition grown two-dimensional (2D) materials. We show that the interplay between the electronic localized states due to edge defects and electron-electron interactions gives rise to local magnetic moments, that break time-reversal symmetry and the topological protection of the edge states in 2D topological systems. Our results suggest that edge disorder leads to small deviations of a perfect quantized conductance in short samples and to a strong conductance suppression in long ones. Our analysis is based on the Kane-Mele model, an unrestricted Hubbard mean-field Hamiltonian, and on a self-consistent recursive Green's function technique to calculate the transport quantities.

DOI: 10.1103/PhysRevB.106.245408

I. INTRODUCTION

The study of topological phenomena has grown enormously over the last years in condensed matter and material sciences, with significant impact in both fundamental and applied research [1–4]. Of particular interest are two-dimensional (2D) topological insulators (TIs) characterized by robust edge states with a helical spin texture. These systems, also called quantum spin Hall (QSH) systems [1,2], are promising platforms for transistor and spintronic applications [4]. Theory predicts that QSH phases require, among other properties, a strong spin-orbit (SO) interaction. The latter can be intrinsic, such as in inverted band semiconductor heterostructures [2] and in a variety of 2D materials [5], or extrinsic, generated by adatom doping [6] or proximity effects [7]. Accordingly, experiments reported QSH realizations in semiconductor quantum wells [8–12], 2D crystals [13–16], and graphene with adsorbed clusters [17].

Time-reversal symmetry and momentum-spin locking make the edge states robust against disorder, preventing backscattering and causing conductance quantization, $\mathcal{G}_0 = 2e^2/h$. There are successful observations of localized edge states [9,18,19] and spin polarization [20] in 2D TIs. However, the unexpected general experimentally determined finite deviations from $\mathcal{G}_0$ in small systems and the conductance suppression in larger samples remain as a long-standing and important puzzle [16,21,22].

The proposed backscattering mechanisms in 2D TIs can be divided into two main categories: interedge hybridization and intraedge spin-flip scattering processes. Since the edge states typically have a penetration depth ξ that is much smaller than the experimental sample widths $\mathcal{W}$, interedge hybridization is usually discarded. However, recent studies speculate that interface roughness in semiconductor heterostructures leads to chiral disorder that can create percolating paths enabling interedge scattering [21]. In turn, since the magnetic impurities are rare in molecular beam epitaxy grown semiconductors as well as in exfoliated 2D materials, the simplest mechanism for spin-flip scattering to explain the lack of topological protection is also ruled out. This motivated several studies to explore a variety of ingenious mechanisms that effectively break time-reversal symmetry, namely, noise [23], edge reconstruction [24], Rashba SO interactions [25,26], phonons [27], nuclear spins [28,29], charge puddles [30], and scattering processes due to adatoms [31], to name a few. Some of those give a temperature dependence at odds with the experimental findings [11,16] and, more importantly, most are only suited for semiconductor heterostructures [8–11]. This study proposes a breakdown of topological protection specific to 2D crystals.

The combination of localization and electron-electron (*e-e*) interactions can also give rise to local magnetic moments. This feature is quite general and has been extensively studied in 2D materials, in particular the properties of vacancy-induced localized states [32–34] and of systems with zigzag terminated edges [35,36]. Recently, Novelli and co-workers [34] have shown that vacancy-induced magnetic moments destroy the topological protection. However, this effect occurs only within narrow energy resonances. Hence, despite being very insightful, this mechanism fails to explain the weak

dependence of the conductance on the gate potential observed in 2D TIs experiments [8–12,16].

In this paper we put forward a nonmagnetic disorder mechanism to explain the breakdown of the topological protection in exfoliated and chemical vapor deposition (CVD) grown 2D materials. We show that edge disorder [37], which is ubiquitous in exfoliated and CVD grown 2D materials, can lead to localization. We find that short sequences of zigzag edge terminations combined with *e-e* interactions drive the formation of local magnetic moments that cause backscattering and destroy the conductance quantization in 2D TIs. We argue that the conductance suppression is small in short samples and can be large in longer ones, in line with experiments.

II. MODEL

We describe the system electronic properties within the topological gap using the Kane-Mele model Hamiltonian with a Hubbard term [34,38]

$$H = H_0 + H_{\rm SO} + H_U. \tag{1}$$

Here, H_0 is the tight-binding Hamiltonian

$$H_0 = -t \sum_{\langle i,j\rangle,\alpha} (c^\dagger_{i\alpha} c_{j\alpha} + \text{H.c.}), \tag{2}$$

where $c^\dagger_{i\alpha}$ ($c_{i\alpha}$) creates (annihilates) an electron of spin α at the honeycomb lattice site i and $\langle i, j\rangle$ limits the hopping integrals to nearest-neighbor sites.

The second term describes the spin-orbit interaction due to adsorbed adatoms [6]

$$H_{\rm SO} = +i\lambda \sum_{\langle\langle i,j\rangle\rangle,\alpha\beta} \nu^p_{ij} c^\dagger_{i\alpha} \sigma^z_{\alpha\beta} c_{i\beta}, \tag{3}$$

where $\boldsymbol{\sigma} = (\sigma^x, \sigma^y, \sigma^z)$ stand for 2×2 Pauli matrices in the spin space, $\langle\langle i, j\rangle\rangle$ restricts the sum to second neighbor sites, and λ is the hopping integral energy. We assume that the adatoms are adsorbed at the so-called hollow positions (centers of the hexagons) of the honeycomb lattice [6], that we denote by p. Accordingly, $\nu^p_{ij} = \pm 1$ distinguishes clockwise ($\nu^p_{ij} = 1$) and counterclockwise ($\nu^p_{ij} = -1$) hopping directions with respect to p if the latter corresponds to an adsorbed adatom position, otherwise $\nu^p_{ij} = 0$. The topological gap Δ_T is proportional to the adatom concentration, namely, $\Delta_T = 6\sqrt{3}\lambda n_{\rm ad}$ [39]. In the limit of $n_{\rm ad} = 1$ all p's are filled and one recovers the original Kane-Mele model [38].

Finally, we account for the *e-e* interaction using an unrestricted Hartree-Fock approximation [40] to the Hubbard Hamiltonian H_U, namely,

$$H^{\rm HF}_U = \frac{U}{2} \sum_{i,\alpha\beta} c^\dagger_{i\alpha} (n_i \mathbf{1}_{\alpha\beta} - \mathbf{m}_i \cdot \boldsymbol{\sigma}_{\alpha\beta}) c_{i\beta} - \frac{U}{4} \sum_i \left(n_i^2 - |\mathbf{m}_i|^2\right), \tag{4}$$

where U represents the on-site (local) *e-e* repulsive interaction, $\mathbf{1}$ is the 2×2 identity matrix, while

$$n_i = \sum_\alpha \langle c^\dagger_{i\alpha} c_{i\alpha}\rangle \tag{5}$$

is the mean electron occupation of the ith site and

$$\mathbf{m}_i = \sum_{\alpha\beta} \langle c^\dagger_{i\alpha} \boldsymbol{\sigma}_{\alpha\beta} c_{i\beta}\rangle \tag{6}$$

is related to the local electronic mean spin polarization, so accordingly we refer to $\mathbf{m}_i$ as local magnetic moments.

We consider a system of width $\mathcal{W}$ and length $\mathcal{L}$ with armchair edges along the transport direction [see Fig. 1(a)]. Left (L) and right (R) contacts connect the system with source and drain reservoirs. For simplicity, we model the contacts by semi-infinite ribbons, with the same width as the central region and doped at $E_F \approx t$ to maximize the number of available propagating modes, mimicking metallic contacts.

III. METHODS

We study the electronic transport using the nonequilibrium Green's function formalism (NEGF) [41–43]. We use the spin-resolved linear conductance $\mathcal{G}_{\alpha\beta}$ as $\mathcal{G}_{\alpha\beta}(\mu) = (e^2/h) \int_{-\infty}^{\infty} (-\partial f_0/\partial E) \mathcal{T}_{\alpha\beta}(E)$, where $f_0(E) = [1 + e^{(E-\mu)/k_BT}]^{-1}$ is the Fermi-Dirac distribution, μ is the equilibrium chemical potential, and $T_{\alpha\beta}$ is the transmission coefficient given by [41]

$$\mathcal{T}_{\alpha\beta}(E) = \text{Tr}[\boldsymbol{\Gamma}_R(E) \mathbf{G}^r_{\alpha\beta}(E) \boldsymbol{\Gamma}_L(E) \mathbf{G}^a_{\beta\alpha}(E)]. \tag{7}$$

Here, $\mathbf{G}^r(E) = [E - \mathbf{H} - \boldsymbol{\Sigma}^r_R(E) - \boldsymbol{\Sigma}^r_L(E)]^{-1}$ and $\mathbf{G}^a(E) = [\mathbf{G}^r(E)]^\dagger$ are, respectively, the retarded and advanced Green's functions in the site representation and $\boldsymbol{\Sigma}^r_{R(L)}$ is the embedding self-energy that depends on the retarded contact Green's functions and the coupling between the contacts $R(L)$ and the central region [42,43]. The R- and L-terminal linewidths are given by $\boldsymbol{\Gamma}_{R(L)}(E) = i[\boldsymbol{\Sigma}^r_{R(L)} - (\boldsymbol{\Sigma}^r_{R(L)})^\dagger]$. Since in our model $\mathcal{T}_{\downarrow\uparrow} = \mathcal{T}_{\uparrow\downarrow} = 0$, the total transmission is $\mathcal{T} = \mathcal{T}_{\uparrow\uparrow} + \mathcal{T}_{\downarrow\downarrow}$.

We also analyze the nonequilibrium local spin-resolved conductance injected by the $R(L)$ terminal $\widetilde{\mathcal{G}}^{R(L)}_{i\alpha,j\beta}$, that is given by $\widetilde{\mathcal{G}}^{R(L)}_{i\alpha,j\beta}(\mu) = (e^2/h) \int_{-\infty}^{\infty} (-\partial f_0/\partial E) \widetilde{\mathcal{T}}^{R(L)}_{i\alpha,j\beta}(E)$, where [44]

$$\widetilde{\mathcal{T}}^{R(L)}_{i\alpha,j\beta}(E) = 2\,\text{Im}[(\mathbf{G}^r \boldsymbol{\Gamma}_{R(L)} \mathbf{G}^a)_{j\beta,i\alpha} H_{i\alpha,j\beta}] \tag{8}$$

is the local transmission of electrons flowing from site j with spin β to the site i with spin α. The spin-resolved local current is obtained using the local version of the Landauer-Büttiker equation $\widetilde{\mathcal{G}}^R_{i\alpha,j\beta} V_R + \widetilde{\mathcal{G}}^L_{i\alpha,j\beta} V_L$, where V_R and V_L are the terminal voltages [44].

We calculate $\mathbf{G}^r$ using the recursive Green's function (RGF) technique [45–47], and $\boldsymbol{\Gamma}_{R,L}(E)$ by decimation [46,48]. The system Green's function depends self-consistently on n_i and $\mathbf{m}_i$ that we obtain using optimized methods (see Supplemental Material [49] and Refs. [50–58] therein for details). For technical reasons [49,59] we perform our calculations at finite temperature keeping $k_BT \ll \Delta_T$, in line with all situations of interest. Hence, in what follows we neglect thermal smearing effects and take $\mu = E_F$.

IV. VACANCY-INDUCED MAGNETIC MOMENTS

The occurrence of vacancies in honeycomb lattices gives rise to quasilocalized states [60–62], For a sufficiently strong *e-e* interaction, due to the Stoner instability, these localized states lead to the formation of local magnetic moments

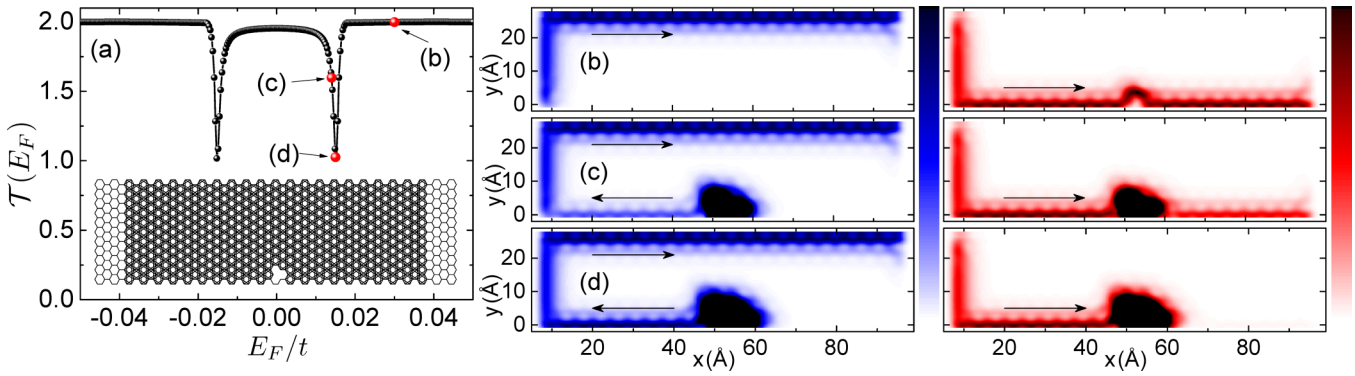

FIG. 1. (a) Total transmission $\mathcal{T}$ as a function of E_F/t. Inset: Sketch of the system geometry with a vacancy close to the bottom edge. Hexagons with lines connecting second neighbor bonds indicate the positions of the adatoms, here $n_{\rm ad} = 1$. Local transmissions injected by the left lead $\mathcal{T}^L_{i\uparrow,j\uparrow}$ (blue) and $\mathcal{T}^L_{i\downarrow,j\downarrow}$ (red) for (b) $E_F = 0.030t$, (c) $E_F = 0.014t$, and (d) $E_F = 0.015t$. The color intensity stands for the magnitude of $\mathcal{T}^L_{i\alpha,j\alpha}$ and the arrows indicate the electron flow direction.

[63–65]. For the Hubbard mean-field approximation, it has been shown that any finite U causes magnetization [66]. Vacancy-induced magnetism has been recently proposed as a mechanism to explain the breakdown of the conductance quantization in TIs [34]. Here, we briefly review this setting and argue that this is hardly a suitable mechanism to explain the lack of conductance quantization observed in experiments.

We consider a system with a vacancy near the bottom edge [see Fig. 1(a)]. We take $\mathcal{W} = 27$ Å, that is sufficiently wide to show no numerical evidence of backscattering due to interedge hybridization. We set $n_{\rm ad} = 1$ and $\lambda = 0.1t$, which leads to $\Delta_T = 1.04t$, and analyze the electronic transport in a chemical potential window within the QSH phase. For these parameters we find enhanced backscattering for $U \gtrsim U^* \approx 0.34t$ [49]. Without loss of generality, we consider $U = 0.4t$. Other values of $U \geqslant U^*$ do not change qualitatively our findings [49].

Figure 1(a) shows the computed total transmission $\mathcal{T}(E_F)$ within the QSH regime. The $\mathcal{T}(E_F)$ is perfectly quantized outside the energy window comprising two narrow antiresonances centered at $\pm E_r$. At the antiresonance there is total backscattering, whereas for E_F between antiresonances $\mathcal{T}(E_F)$ is slightly suppressed with respect to $\mathcal{T} = 2$.

The involved scattering processes can be qualitatively understood by analyzing the local transmissions shown in Figs. 1(b)–1(d). For $E_F = 0.030t$ the total transmission is quantized, and the electrons injected by the L terminal are transmitted by the helical edge states without backscattering [see Fig. 1(b)]. For $E_F = 0.014t$ the transmission is no longer perfect. The local magnetic moment at the sites around the vacancy cause a spin-flip process enabling partial backscattering that reduces the $L \to R$ transmission of spin-down electrons [see Fig. 1(c)]. This situation becomes more dramatic at the antiresonance peak $E_F = E_r = 0.015t$, for which the $L \to R$ transmission of spin-down electrons is fully blocked [see Fig. 1(d)].

The magnetization around the vacancy decays as a power law [62,67], that explains the relatively large regions over which the edge currents invert their direction of propagation [see Figs. 1(c) and 1(d)]. Note that the edge states decay exponentially towards the bulk with a penetration depth $\xi = \hbar v_F/\Delta_T$, suppressing the spin-flip coupling as the vacancy is moved away from the edge.

The observed features can be quantitatively described by an effective single-edge low-energy model with a Hilbert space that consists of the vacancy-induced quasilocalized state $|0\rangle$ at $E = 0$ [61] and helical edge modes ($|k,\uparrow\rangle$ and $|-k,\downarrow\rangle$). This simplification allows one to map the microscopic problem into the model of an edge state scattered by a short-range magnetic impurity proposed in Ref. [32]. The analytical solution [32,33] of the corresponding Lippmann-Schwinger equation gives a single-edge transmission that is very similar to that of Fig. 1(a). A detailed comparison between the microscopic and the effective model shows that a strong conductance suppression is always associated with resonance processes with narrow energy decay widths Γ, namely, $\Gamma/\Delta_T \ll 1$ [49].

We conclude that vacancies are unlikely to explain the breakdown of conductance quantization observed in experiments, since (i) vacancies have low concentrations in good quality samples, (ii) the model requires that the vacancies occur very close to the system edges (within the edge state penetration depth), and (iii) the conductance suppression occurs only over a very narrow chemical potential doping window, a feature that has not been observed in experiments. Diluted distributed vacancies are hardly expected to modify this scenario.

V. WEDGE DEFECT

Local magnetic moments can also be originated by *e-e* interactions in localized states due to the system edge terminations. This subject has been extensively investigated in graphene zigzag [63,68] and chiral [69] nanoribbons. Interestingly, it has been theoretically shown that a small sequence of zigzag links is sufficient to spin polarize the system for any finite U [35,70]. Let us study the simplest lattice edge geometry that leads to the formation of a local magnetic moment for our model Hamiltonian, Eq. (1): a wedge or V-shaped defect. We note that a similar kind of edge defect has been recently observed experimentally in high-precision bottom-up nanoribbon graphene synthesis [36].

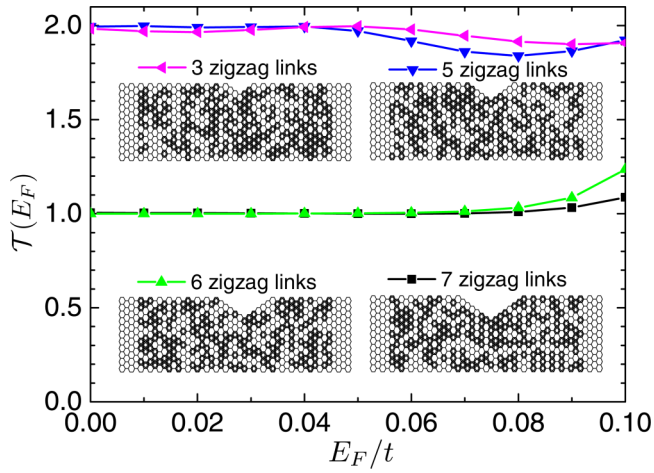

FIG. 2. Total transmission $\mathcal{T}(E_F)$ for wedge-shaped edge defects of different lengths. The insets show wedge defects with $\ell = 3, 5, 6,$ and 7 zigzag links. The darker sites correspond to the hexagons with adsorbed adatoms, in all cases $n_{\rm ad} = 0.5$.

Now we take $n_{\rm ad} = 0.5$, $\lambda = 0.1t$, and keep $\mathcal{W} = 27$ Å, that is sufficiently wide to prevent interedge scattering and exhibits perfect conductance quantization for $U = 0$. Figure 2 shows the total transmission $\mathcal{T}$ as a function of E_F/t for $U = t$. For small zigzag wedges, $\ell = 3$ and $\ell = 5$ links long, the transmission is already no longer quantized and the deviation from perfect transmission shows a tendency to increase with E_F. Remarkably, there is a sharp transition for zigzag wedges with $\ell = 6$ links and longer: The transmission along the edge with the V-shape defect becomes zero over a large fraction of the topological gap energy window.

Here, the localized edge states are very different from the vacancy-induced ones and so is the local magnetization. We find that the in-plane magnetic moments are strongly peaked and almost constant along the ℓ zigzag chain at the system edge and show a fast decay for sites with increasing distance to the edge [49]. The local transmissions show that the spin-flip processes occur in the vicinity of the wedge defect, suggesting that $\delta w/\xi \gtrsim 1$, where δw is the depth of the wedge, is required to maximize the effect. For the parameters we consider, the latter inequality implies $\ell \gtrsim 5$, consistent with Fig. 2.

VI. ROUGH EDGE DISORDER

Let us now study a more realistic edge disorder model. Both for lithographic and CVD synthesized samples, the system edges can be assumed as rough, with no clear crystallographic orientation. Nonetheless, experiments show [71,72] that experimental samples do display sequences of zigzag and armchair links. Below, we investigate the impact of edge roughness on the wedge-defect-induced magnetic moments.

The inset at the bottom of Fig. 3(a) shows a realization of rough edge disorder. We consider a system with a single wedge defect and generate the edge disorder by randomly removing atoms from the two hexagonal rows at the system top edge. Next, we remove any atom forming dangling bonds. We find that the edge roughness increases the edge states' penetration depth ξ. We increase the system width to $\mathcal{W} \approx 57$ Å to prevent interedge scattering. The inset at the top of Fig. 3(a) shows the corresponding m_{ix} at $E_F = 0$ and indicates that the presence of edge roughness does not break the wedge-defect-induced magnetization. As expected, we find that the magnetization of longer zigzag chains ℓ is stronger than that of sequences with a smaller ℓ.

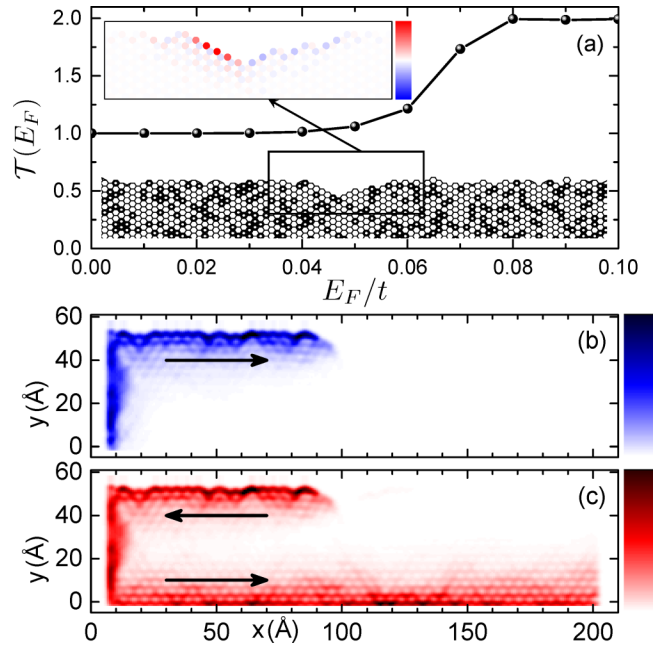

FIG. 3. (a) Total transmission $\mathcal{T}(E_F)$ for the disorder realization and local moment shown in the lower and upper insets. Local transmission $\widetilde{\mathcal{T}}^{L}_{i\alpha,j\alpha}(E_F = 0)$ in arbitrary units for (b) for spin-up ($\alpha = \uparrow$) and (c) spin-down ($\alpha = \downarrow$) electrons.

Figure 3(a) shows $\mathcal{T}(E_F)$ for the disorder realization presented in the inset. Due to edge roughness, backscattering is slightly suppressed as compared to Fig. 2, but the qualitative behavior is similar: The transmission through the top edge goes to zero over a wide Fermi energy window inside the topological gap, remaining finite for other values of E_F. Figure 3(b) shows $\widetilde{\mathcal{T}}^{L}_{i\alpha,j\alpha}(E_F = 0)$. Spin-up electrons flowing from L to R are scattered by the local magnetic moment [see the upper inset of Fig. 3(a)] that flips their spins and forces them to propagate back to the L terminal, as displayed by Figs. 3(b) and 3(c) at $E_F = 0$. The propagation from L to R at the bottom edge has perfect transmission.

Clearly, the probability for the occurrence of long zigzag chains is smaller than that of short ones. The picture that emerges is as follows: Systems with small $\mathcal{L}$ are dominated by short ℓ wedge defects that lead to small deviations from conductance quantization, $2 - \mathcal{T} \ll 1$. With increasing $\mathcal{L}$, wedge defects with $\ell > 5$ are more likely to occur, resulting in a strong suppression of $\mathcal{T}$.

VII. SUMMARY

We have studied the suppression of the conductance quantization in exfoliated and CVD grown 2D materials in the QSH regime due to local magnetic moments caused by edge disorder, that is ubiquitous in such systems. We find that the interplay between a single wedge defect and *e-e* interactions

can destroy topological protection over a large extension of the topological gap, either causing a small modification in the conductance quantization or strongly suppressing the conductance. We conjecture that the latter is more likely to occur in large samples. We believe that this mechanism is quite general and applicable to a large variety of intrinsic 2D topological insulators as well as for extrinsic adatom doped and proximity 2D TIs.

ACKNOWLEDGMENTS

The authors acknowledge the financial support of the Brazilian funding agencies CNPq, FAPERJ, and the Brazilian Institute of Science and Technology (INCT) in Carbon Nanomaterials. The simulations were partially performed at NACAD-COPPE/Federal University of Rio de Janeiro, Brazil.

[1] M. Z. Hasan and C. L. Kane, Colloquium: Topological insulators, Rev. Mod. Phys. **82**, 3045 (2010).
[2] X.-L. Qi and S.-C. Zhang, Topological insulators and superconductors, Rev. Mod. Phys. **83**, 1057 (2011).
[3] Y. Ren, Z. Qiao, and Q. Niu, Topological phases in two-dimensional materials: a review, Rep. Prog. Phys. **79**, 066501 (2016).
[4] D. Culcer, A. C. Keser, Y. Li, and G. Tkachov, Transport in two-dimensional topological materials: recent developments in experiment and theory, 2D Mater. **7**, 022007 (2020).
[5] A. Marrazzo, M. Gibertini, D. Campi, N. Mounet, and N. Marzari, Relative abundance of $\mathbb{Z}_2$ topological order in exfoliable two-dimensional insulators, Nano Lett. **19**, 8431 (2019).
[6] C. Weeks, J. Hu, J. Alicea, M. Franz, and R. Wu, Engineering a Robust Quantum Spin Hall State in Graphene via Adatom Deposition, Phys. Rev. X **1**, 021001 (2011).
[7] A. Avsar, H. Ochoa, F. Guinea, B. Özyilmaz, B. J. van Wees, and I. J. Vera-Marun, Colloquium: Spintronics in graphene and other two-dimensional materials, Rev. Mod. Phys. **92**, 021003 (2020).
[8] M. König, S. Wiedmann, C. Brüne, A. Roth, H. Buhmann, L. W. Molenkamp, X.-L. Qi, and S.-C. Zhang, Quantum spin Hall insulator state in HgTe quantum wells, Science **318**, 766 (2007).
[9] A. Roth, C. Brüne, H. Buhmann, L. W. Molenkamp, J. Maciejko, X.-L. Qi, and S.-C. Zhang, Nonlocal transport in the quantum spin Hall state, Science **325**, 294 (2009).
[10] G. M. Gusev, Z. D. Kvon, O. A. Shegai, N. N. Mikhailov, S. A. Dvoretsky, and J. C. Portal, Transport in disordered two-dimensional topological insulators, Phys. Rev. B **84**, 121302(R) (2011).
[11] I. Knez, C. T. Rettner, S.-H. Yang, S. S. P. Parkin, L. Du, R.-R. Du, and G. Sullivan, Observation of Edge Transport in the Disordered Regime of Topologically Insulating InAs/GaSb Quantum Wells, Phys. Rev. Lett. **112**, 026602 (2014).
[12] L. Du, I. Knez, G. Sullivan, and R.-R. Du, Robust Helical Edge Transport in Gated InAs/GaSb Bilayers, Phys. Rev. Lett. **114**, 096802 (2015).
[13] F. Reis, G. Li, L. Dudy, M. Bauernfeind, S. Glass, W. Hanke, R. Thomale, J. Schäfer, and R. Claessen, Bismuthene on a SiC substrate: A candidate for a high-temperature quantum spin Hall material, Science **357**, 287 (2017).
[14] X.-B. Li, W.-K. Huang, Y.-Y. Lv, K.-W. Zhang, C.-L. Yang, B.-B. Zhang, Y. B. Chen, S.-H. Yao, J. Zhou, M.-H. Lu, L. Sheng, S.-C. Li, J.-F. Jia, Q.-K. Xue, Y.-F. Chen, and D.-Y. Xing, Experimental Observation of Topological Edge States at the Surface Step Edge of the Topological Insulator $ZrTe_5$, Phys. Rev. Lett. **116**, 176803 (2016).
[15] Z. Fei, T. Palomaki, S. Wu, W. Zhao, X. Cai, B. Sun, P. Nguyen, J. Finney, X. Xu, and D. H. Cobden, Edge conduction in monolayer WTe_2, Nat. Phys. **13**, 677 (2017).
[16] S. Wu, V. Fatemi, Q. D. Gibson, K. Watanabe, T. Taniguchi, R. J. Cava, and P. Jarillo-Herrero, Observation of the quantum spin Hall effect up to 100 kelvin in a monolayer crystal, Science **359**, 76 (2018).
[17] K. Hatsuda, H. Mine, T. Nakamura, J. Li, R. Wu, S. Katsumoto, and J. Haruyama, Evidence for a quantum spin Hall phase in graphene decorated with Bi_2Te_3 nanoparticles, Sci. Adv. **4**, eaau6915 (2018).
[18] K. C. Nowack, E. M. Spanton, M. Baenninger, M. König, J. R. Kirtley, B. Kalisky, C. Ames, P. Leubner, C. Brüne, H. Buhmann, L. W. Molenkamp, D. Goldhaber-Gordon, and K. A. Moler, Imaging currents in HgTe quantum wells in the quantum spin Hall regime, Nat. Mater. **12**, 787 (2013).
[19] K. Suzuki, Y. Harada, K. Onomitsu, and K. Muraki, Edge channel transport in the InAs/GaSb topological insulating phase, Phys. Rev. B **87**, 235311 (2013).
[20] C. Brüne, A. Roth, H. Buhmann, E. M. Hankiewicz, L. W. Molenkamp, J. Maciejko, X.-L. Qi, and S.-C. Zhang, Spin polarization of the quantum spin Hall edge states, Nat. Phys. **8**, 485 (2012).
[21] L. Lunczer, P. Leubner, M. Endres, V. L. Müller, C. Brüne, H. Buhmann, and L. W. Molenkamp, Approaching Quantization in Macroscopic Quantum Spin Hall Devices through Gate Training, Phys. Rev. Lett. **123**, 047701 (2019).
[22] C.-H. Hsu, P. Stano, J. Klinovaja, and D. Loss, Helical liquids in semiconductors, Semicond. Sci. Technol. **36**, 123003 (2021).
[23] J. I. Väyrynen, D. I. Pikulin, and J. Alicea, Noise-Induced Backscattering in a Quantum Spin Hall Edge, Phys. Rev. Lett. **121**, 106601 (2018).
[24] J. Wang, Y. Meir, and Y. Gefen, Spontaneous Breakdown of Topological Protection in Two Dimensions, Phys. Rev. Lett. **118**, 046801 (2017).
[25] A. Ström, H. Johannesson, and G. I. Japaridze, Edge Dynamics in a Quantum Spin Hall State: Effects from Rashba Spin-Orbit Interaction, Phys. Rev. Lett. **104**, 256804 (2010).
[26] J. R. Bindel, M. Pezzotta, J. Ulrich, M. Liebmann, E. Ya. Sherman, and M. Morgenstern, Probing variations of the Rashba spin-orbit coupling at the nanometre scale, Nat. Phys. **12**, 920 (2016).
[27] J. C. Budich, F. Dolcini, P. Recher, and B. Trauzettel, Phonon-Induced Backscattering in Helical Edge States, Phys. Rev. Lett. **108**, 086602 (2012).
[28] C.-H. Hsu, P. Stano, J. Klinovaja, and D. Loss, Effects of nuclear spins on the transport properties of the edge of two-

dimensional topological insulators, Phys. Rev. B **97**, 125432 (2018).
[29] A. A. Bagrov, F. Guinea, and M. I. Katsnelson, Suppressing backscattering of helical edge modes with a spin bath, Phys. Rev. B **100**, 195426 (2019).
[30] J. I. Väyrynen, M. Goldstein, and L. I. Glazman, Helical Edge Resistance Introduced by Charge Puddles, Phys. Rev. Lett. **110**, 216402 (2013).
[31] F. J. Santos, D. A. Bahamon, R. B. Muniz, K. McKenna, E. V. Castro, J. Lischner, and A. Ferreira, Impact of complex adatom-induced interactions on quantum spin Hall phases, Phys. Rev. B **98**, 081407(R) (2018).
[32] X. Dang, J. D. Burton, and E. Y. Tsymbal, Magnetic gating of a 2D topological insulator, J. Phys.: Condens. Matter **28**, 38LT01 (2016).
[33] J.-H. Zheng and M. A. Cazalilla, Nontrivial interplay of strong disorder and interactions in quantum spin-Hall insulators doped with dilute magnetic impurities, Phys. Rev. B **97**, 235402 (2018).
[34] P. Novelli, F. Taddei, A. K. Geim, and M. Polini, Failure of Conductance Quantization in Two-Dimensional Topological Insulators due to Nonmagnetic Impurities, Phys. Rev. Lett. **122**, 016601 (2019).
[35] M. Wimmer, I. Adagideli, S. Berber, D. Tománek, and K. Richter, Spin Currents in Rough Graphene Nanoribbons: Universal Fluctuations and Spin Injection, Phys. Rev. Lett. **100**, 177207 (2008).
[36] M. Pizzochero, G. B. Barin, K. Čerņevivs, S. Wang, P. Ruffieux, R. Fasel, and O. V. Yazyev, Edge disorder in bottom-up zigzag graphene nanoribbons: Implications for magnetism and quantum electronic transport, J. Phys. Chem. Lett. **12**, 4692 (2021).
[37] E. R. Mucciolo, A. H. Castro Neto, and C. H. Lewenkopf, Conductance quantization and transport gaps in disordered graphene nanoribbons, Phys. Rev. B **79**, 075407 (2009).
[38] C. L. Kane and E. J. Mele, Quantum Spin Hall Effect in Graphene, Phys. Rev. Lett. **95**, 226801 (2005).
[39] O. Shevtsov, P. Carmier, C. Petitjean, C. Groth, D. Carpentier, and X. Waintal, Graphene-Based Heterojunction between Two Topological Insulators, Phys. Rev. X **2**, 031004 (2012).
[40] Some authors (see, for instance, Ref. [22] for a review) address the scenario where the *e-e* interaction drives the helical edge modes into a Luttinger liquid. A consistent theory [22] requires a Luttinger liquid parameter that corresponds to a strong *e-e* interaction, which is not supported by experimental evidence, with the possible exception of InAs/GaSb quantum wells.
[41] Y. Meir and N. S. Wingreen, Landauer Formula for the Current Through an Interacting Electron Region, Phys. Rev. Lett. **68**, 2512 (1992).
[42] S. Datta, *Electronic Transport in Mesoscopic Systems* (Cambridge University Press, Cambridge, UK, 1995).
[43] H. Haug and A. J. Jauho, *Quantum Kinetics in Transport and Optics of Semiconductors*, Solid-State Sciences Vol. 123 (Springer, Heidelberg, 2008).
[44] L. R. F. Lima and C. Lewenkopf, Local equilibrium charge and spin currents in two-dimensional topological systems, Phys. Rev. B **105**, 085420 (2022).
[45] A. MacKinnon, The calculation of transport properties and density of states of disordered solids, Z. Phys. B **59**, 385 (1985).
[46] C. H. Lewenkopf and E. R. Mucciolo, The recursive Green's function method for graphene, J. Comput. Electron. **12**, 203 (2013).
[47] L. R. F. Lima, A. Dusko, and C. Lewenkopf, Efficient method for computing the electronic transport properties of a multiterminal system, Phys. Rev. B **97**, 165405 (2018).
[48] M. P. Lopez Sancho, J. M. Lopez Sancho, and J. Rubio, Highly convergent schemes for the calculation of bulk and surface Green functions, J. Phys. F: Met. Phys. **15**, 851 (1985).
[49] See Supplemental Material at http://link.aps.org/supplemental/10.1103/PhysRevB.106.245408 for additional information on the numerical method and for results of the vacancy- and wedge-defect-induced local magnetic moments.
[50] T. Ozaki, Continued fraction representation of the Fermi-Dirac function for large-scale electronic structure calculations, Phys. Rev. B **75**, 035123 (2007).
[51] A. Croy and U. Saalmann, Partial fraction decomposition of the Fermi function, Phys. Rev. B **80**, 073102 (2009).
[52] D. A. Areshkin and B. K. Nikolić, Electron density and transport in top-gated graphene nanoribbon devices: First-principles Green function algorithms for systems containing a large number of atoms, Phys. Rev. B **81**, 155450 (2010).
[53] D. Singh, H. Krakauer, and C. S. Wang, Accelerating the convergence of self-consistent linearized augmented-plane-wave calculations, Phys. Rev. B **34**, 8391 (1986).
[54] S. Ihnatsenka, I. V. Zozoulenko, and M. Willander, Electron-electron interaction effects in transport through open dots: Pinning of resonant levels, Phys. Rev. B **75**, 235307 (2007).
[55] A. M. Valencia and M. J. Caldas, Single vacancy defect in graphene: Insights into its magnetic properties from theoretical modeling, Phys. Rev. B **96**, 125431 (2017).
[56] A. Pezo, B. Focassio, G. R. Schleder, M. Costa, C. Lewenkopf, and A. Fazzio, Disorder effects of vacancies on the electronic transport properties of realistic topological insulator nanoribbons: The case of bismuthene, Phys. Rev. Mater. **5**, 014204 (2021).
[57] H.-Y. Deng and K. Wakabayashi, Edge effect on a vacancy state in semi-infinite graphene, Phys. Rev. B **90**, 115413 (2014).
[58] T. O. Wehling, E. Şaşıoğlu, C. Friedrich, A. I. Lichtenstein, M. I. Katsnelson, and S. Blügel, Strength of Effective Coulomb Interactions in Graphene and Graphite, Phys. Rev. Lett. **106**, 236805 (2011).
[59] L. R. F. Lima and C. H. Lewenkopf, Disorder-assisted transmission due to charge puddles in monolayer graphene: Transmission enhancement and local currents, Phys. Rev. B **93**, 045404 (2016).
[60] E. H. Lieb, Two Theorems on the Hubbard Model, Phys. Rev. Lett. **62**, 1201 (1989).
[61] V. M. Pereira, J. M. B. Lopes dos Santos, and A. H. Castro Neto, Modeling disorder in graphene, Phys. Rev. B **77**, 115109 (2008).
[62] B. R. K. Nanda, M. Sherafati, Z. S. Popović, and S. Satpathy, Electronic structure of the substitutional vacancy in graphene: density-functional and Green's function studies, New J. Phys. **14**, 083004 (2012).
[63] O. V. Yazyev, Emergence of magnetism in graphene materials and nanostructures, Rep. Prog. Phys. **73**, 056501 (2010).

[64] M. M. Ugeda, I. Brihuega, F. Guinea, and J. M. Gómez-Rodríguez, Missing Atom as a Source of Carbon Magnetism, Phys. Rev. Lett. **104**, 096804 (2010).

[65] Y. Zhang, S.-Y. Li, H. Huang, W.-T. Li, J.-B. Qiao, W.-X. Wang, L.-J. Yin, K.-K. Bai, W. Duan, and L. He, Scanning Tunneling Microscopy of the π Magnetism of a Single Carbon Vacancy in Graphene, Phys. Rev. Lett. **117**, 166801 (2016).

[66] H. Kumazaki and D. S. Hirashima, Nonmagnetic-defect-induced magnetism in graphene, J. Phys. Soc. Jpn. **76**, 064713 (2007).

[67] V. G. Miranda, L. G. G. V. Dias da Silva, and C. H. Lewenkopf, Coulomb charging energy of vacancy-induced states in graphene, Phys. Rev. B **94**, 075114 (2016).

[68] Y.-W. Son, M. L. Cohen, and S. G. Louie, Half-metallic graphene nanoribbons., Nature (London) **444**, 347 (2006).

[69] C. Tao, L. Jiao, O. V. Yazyev, Y.-C. Chen, J. Feng, X. Zhang, R. B. Capaz, J. M. Tour, A. Zettl, S. G. Louie, H. Dai, and M. F. Crommie, Spatially resolving edge states of chiral graphene nanoribbons, Nat. Phys. **7**, 616 (2011).

[70] H. Kumazaki and D. S. Hirashima, Local magnetic moment formation on edges of graphene, J. Phys. Soc. Jpn. **77**, 044705 (2008).

[71] X. Zhang, O. V. Yazyev, J. Feng, L. Xie, C. Tao, Y.-C. Chen, L. Jiao, Z. Pedramrazi, A. Zettl, S. G. Louie, H. Dai, and M. F. Crommie, Experimentally engineering the edge termination of graphene nanoribbons, ACS Nano **7**, 198 (2013).

[72] P. Leicht, L. Zielke, S. Bouvron, R. Moroni, E. Voloshina, L. Hammerschmidt, Y. S. Dedkov, and M. Fonin, *In situ* fabrication of quasi-free-standing epitaxial graphene nanoflakes on gold, ACS Nano **8**, 3735 (2014).